Clim. Past Discuss., 10, 2979–3026, 2014
www.clim-past-discuss.net/10/2979/2014/
doi:10.5194/cpd-10-2979-2014
© Author(s) 2014. CC Attribution 3.0 License.

Climate of the Past Discussions
Open Access

This discussion paper is/has been under review for the journal Climate of the Past (CP). Please refer to the corresponding final paper in CP if available.

Changes in Mediterranean circulation and water characteristics due to restriction of the Atlantic connection: a high-resolution parallel ocean model

R. P. M. Topper[1,*] and P. Th. Meijer[1]

[1]Department of Earth Sciences, Utrecht University, Budapestlaan 4 3584CD Utrecht, the Netherlands
[*]now at: MARUM – Center for Marine Environmental Sciences and Department of Geosciences, University of Bremen, P.O. Box 33 04 40, 28334, Germany

Received: 27 June 2014 – Accepted: 13 July 2014 – Published: 25 July 2014

Correspondence to: R. P. M. Topper (rtopper@marum.de)

Published by Copernicus Publications on behalf of the European Geosciences Union.

cc BY

Abstract

A high-resolution parallel ocean model is set up to examine how the sill depth of the Atlantic connection affects circulation and water characteristics in the Mediterranean Basin. An analysis of the model performance, comparing model results with observations on the present-day Mediterranean, demonstrates its ability to reproduce observed water characteristics and circulation (including deep water formation). A series of experiments with different sill depths in the Atlantic–Mediterranean connection is used to assess the sensitivity of Mediterranean circulation and water characteristics to sill depth. Basin-averaged water salinity and, to a lesser degree, temperature rise when the sill depth is less and exchange with the Atlantic is lower. Lateral and interbasinal differences in the Mediterranean are, however, largely unchanged. The strength of the upper overturning cell in the western basin is proportional to the magnitude of the exchange with the Atlantic, and hence to sill depth. Overturning in the eastern basin and deep water formation in both basins, on the contrary, are little affected by the sill depth.

The model results are used to interpret the sedimentary record of the Late Miocene preceding and during the Messinian Salinity Crisis. In the western basin a correlation exists between sill depth and rate of refreshment of deep water. On the other hand, because sill depth has little effect on the overturning and deep water formation in the eastern basin, the model results do not support the notion that restriction of the Atlantic–Mediterranean connection may cause lower oxygenation of deep water in the eastern basin. However, this discrepancy may be due to simplifications in the surface forcing and the use of a bathymetry different from that in the Late Miocene. We also tentatively conclude that blocked outflow, as found in experiments with a sill depth ≤ 10 m, is a plausible scenario for the second stage of the Messinian Salinity Crisis during which halite was rapidly accumulated in the Mediterranean.

With the model setup and experiments, a basis has been established for future work on the sensitivity of Mediterranean circulation to changes in (palaeo-)bathymetry and external forcings.

CPD
10, 2979–3026, 2014

CC BY

1 Introduction

Ever since the closure of the connection to the Indian Ocean in the Middle Miocene, water exchange between the Mediterranean Sea and the global ocean has been through one or multiple gateways in the Gibraltar arc (e.g. Dercourt et al., 2000). In the Mediterranean, the water loss by evaporation exceeds, on an annual basis, the fresh water input from precipitation and river input. The resulting fresh water deficit, i.e. evaporation – precipitation – river input, is compensated by a net inflow from the Atlantic. Without a connection to the global ocean, the deficit would not be replenished and Mediterranean sea level would rapidly drop (Meijer and Krijgsman, 2005). At present, the fresh water deficit in combination with the relatively small connection to the Atlantic results in a higher salinity in the Mediterranean than in the Atlantic. This salinity difference, and hence density difference, between the Mediterranean and Atlantic drives a deep outflow of Mediterranean water. The outflow is compensated for with an inflow of less saline Atlantic water at the surface (e.g. Bryden and Kinder, 1991; Astraldi et al., 1999).

This pattern of surface inflow and deep outflow is known as anti-estuarine and has been the dominant mode of exchange since at least the closure of the Indian Ocean connection (Karami et al., 2011; Seidenkrantz et al., 2000; de la Vara et al., 2014). On a geological time scale, the fresh water budget of the Mediterranean has changed in accord with global climate. Superimposed on long term variations are orbitally driven changes on shorter timescales. Precession and eccentricity have been shown to have a significant impact on Mediterranean river discharge, evaporation and precipitation (e.g. Tuenter et al., 2003). Due to the small exchange with the Atlantic, precessional changes in the fresh water budget have a pronounced effect on the Mediterranean circulation. The Mediterranean sedimentary record contains evidence for reduced bottom water ventilation during periods of precession-induced increased river discharge in the form of sapropels since the Miocene (Hilgen et al., 1995; Cramp and O'Sullivan, 1999).

In the Neogene and Quarternary sedimentary record, the occurrence of sapropels has been related to relatively strong precession minima, clustered in intervals

CPD
10, 2979–3026, 2014

cc BY

with particularly high eccentricity (100 and 400 kyr cycle). However, at the end of the Miocene (7.16–5.332 Ma), sapropels were formed in nearly every precession cycle (Seidenkrantz et al., 2000), indicative of a heightened sensitivity of Mediterranean circulation to its fresh water budget. Within an interval of increasing bottom water salinity starting at ≈ 8 Ma, a sharp change in the foraminiferal assemblage and a shift in δ^{13}C at 7.16 Ma indicate reduced bottom water ventilation in several relatively deep marginal basins of the Mediterranean (Seidenkrantz et al., 2000; Kouwenhoven et al., 2003; Kouwenhoven and van der Zwaan, 2006). Low oxygen and high salinity conditions expand from deep marginal basins to marginal basins at shallower depths towards the onset of the Messinian Salinity Crisis (Gennari et al., 2013). The concurrent increase in sensitivity to changes in the fresh water budget, the increase in salinity, and the drop in bottom water ventilation, have been interpreted as indicators of reduced exchange with the Atlantic due to restriction of the Atlantic–Mediterranean connection (Kouwenhoven and van der Zwaan, 2006).

The ultimate expression of a strong restriction in Atlantic–Mediterranean exchange is the Messinian Salinity Crisis (MSC), an event which is represented in the sedimentary record by widespread and voluminous evaporites in the Mediterranean. Circum-Mediterranean climate changed little during this event (Fauquette et al., 2006; Bertini, 2006), corroborating the results of model studies that demonstrate that a restriction of the Atlantic–Mediterranean connection can be the sole driver of the MSC (Topper et al., 2011; Topper and Meijer, 2013). A vast halite layer (1–2 km in the deep basins) formed during the short second phase of the Messinian Salinity Crisis (5.61–5.55 Ma, Roveri and Manzi, 2006). A scenario with inflow from the Atlantic but no outflow, the so-called block-outflow scenario, has been proposed to explain the fast accumulation of salt in the Mediterranean (Krijgsman et al., 1999a; Meijer, 2006; Krijgsman and Meijer, 2008). According to hydraulic control theory, blocked outflow can be attained in the Atlantic–Mediterranean gateway when the water depth is just a few meters (Meijer, 2012).

CPD
10, 2979–3026, 2014

CC BY

In the Late Miocene, Atlantic–Mediterranean exchange occurred through two shallow marine gateways in northern Morocco and southern Spain, respectively the Rifian and Betic corridors (Benson et al., 1991; Betzler et al., 2006). Due to their geometry, i.e. shallow, wide and long, and position at the interface of ongoing Africa–Eurasia convergence, these gateways were vulnerable to changes in width and depth by tectonics (Duggen et al., 2003; Weijermars, 1988; Govers, 2009). Opening and closure of both gateways is recorded in the sedimentary record of the subbasins that make up the corridors. Closure of the Rifian corridor took place somewhere in the interval 6.8–6.0 Ma (Krijgsman et al., 1999b; Ivanovic et al., 2013; van Assen et al., 2006).The Betic corridor has long thought to be closed by 7.8 Ma (Soria et al., 1999; Betzler et al., 2006; Martín et al., 2009). Recent work has disputed this, stating that the Betic corridor might have been open after 7.8 Ma (Hüsing et al., 2010; Pérez-Asensio et al., 2012). Wherever the connection may have been, the volume of evaporites formed during the MSC can only be explained by a continued inflow of saline water from the Atlantic (Sonnenfeld and Finetti, 1985; Krijgsman and Meijer, 2008; Topper and Meijer, 2013).

The purpose of this study is to examine with a high-resolution ocean circulation model how sill depth of the Atlantic connection affects circulation and water characteristics in the Mediterranean Basin. The physics-based insight thus gained is used to evaluate the Late Miocene sedimentary record: that of the Messinian Salinity Crisis and, in particular, that of the period just preceding the actual crisis. Notwithstanding our focus on the Late Miocene, the basin bathymetry is – except near the Atlantic connection – that of the present Mediterranean Sea. The reasons for this are that (1) we isolate the changes in circulation and water characteristics that are caused by a different depth of the Atlantic connection, and (2) a validation of model performance is only possible in a present-day model setup because quantitative data on water properties and circulation does not exist for other time periods. Such an assessment of model performance is necessary because the model has not been applied to the Mediterranean before. Thus taking the present-day bathymetry as our reference, the depth of the Strait of Gibraltar is modified to gain insight into the role of depth of the Atlantic connection.

CPD
10, 2979–3026, 2014

CC BY

Even though basin shape was different in the Late Miocene and the connection to the ocean had a different geometry and location, our model results form a good starting point for this past time as well. The reason for this is that, in terms of features that govern the overall circulation and water properties, the present-day and Late Miocene basin geometry are largely similar. Both consist of two sub-basins, comprise limited shelf areas and deep-basinal portions, are subject to net evaporation and posses parts located at relatively high latitude where cooling of the surface water occurs. Thus, insight gained about the change in circulation and water properties due to variation in sill depth is expected to be largely generic. A minimal model of the Mediterranean with a highly idealized surface forcing has been shown to be able to capture the important characteristics of Mediterranean circulation (Meijer and Dijkstra, 2009). A similar idealized surface forcing is applied in this study, a simplification of the model setup that is justified when the focus is on the influence of the sill depth.

Water exchange in the present-day Strait of Gibraltar has been studied extensively because of its influence on Mediterranean water characteristics and, therewith, circum-Mediterranean climate (Bryden and Stommel, 1984; Sannino et al., 2002; Astraldi et al., 1999; Hopkins, 1999; Candela, 1991; Bryden et al., 1994). The present-day Mediterranean circulation and the influence of temporal variations in the surface forcing, e.g. fresh water budget and heat flux, has also been widely studied, often in the context of sapropels (Meijer and Tuenter, 2007; Meijer and Dijkstra, 2009; Samuel et al., 1999; Myers et al., 1998b, a; Myers, 2002). Data and simple modelling studies have demonstrated the importance of the size of the Atlantic–Mediterranean connection in controlling sedimentation and circulation in the Mediterranean. Recently, ocean circulation models have been used to investigate the influence of gateway geometry on water characteristics and circulation in an idealized marginal basin (Iovino et al., 2008; Pratt and Spall, 2008) and realistic marginal basins, e.g. the Miocene Arctic Ocean (Thompson et al., 2010). Similar studies, regarding the influence of gateway geometry on Mediterranean circulation and water characteristics, are, as yet, few in number. The sensitivity of circulation in the Late Miocene Mediterranean to changes in the palaeo-

CPD
10, 2979–3026, 2014

R. P. M. Topper and P. Th. Meijer

CC BY

geography has been examined by Meijer et al. (2004). More recently, Alhammoud et al. (2010) have examined how the sill depth of the Strait of Gibraltar affects the thermohaline circulation in a highly idealized coarse resolution ocean circulation model.

The next section will provide a description of the model and boundary conditions used. In Sect. 3, the results of a reference experiment with the present-day sill depth will be compared to water characteristics and circulation as observed or modelled for the present-day Mediterranean to assess model performance. Keeping all other boundary conditions constant, the sill depth of the Atlantic gateway will be both increased, up to 500 m, and reduced, down to 5 m, in a series of experiments. Model results will be discussed in the context of the Late Miocene restriction of the Atlantic–Mediterranean connection and the blocked-outflow scenario for the Messinian Salinity Crisis.

2 Model description

For a good representation of water exchange through a shallow gateway, a model with a high number of vertical layers in shallow water is required. A model with vertical sigma coordinates meets this requirement better than a model with z coordinates. With sigma coordinates, regardless of water depth, the number of vertical gridpoints in the water column is equal. The distance between vertical gridpoints is a constant percentage of the total waterdepth at each point, i.e. layers are further apart in deep water than in shallow water. In this study, we use sbPOM (Jordi and Wang, 2012), a recently developed parallel, free-surface, sigma-coordinate, primitive equations ocean modelling code based on the Princeton Ocean Model (Blumberg and Mellor, 1987). Differences between sbPOM and the 2008 version of POM only concern the parallelisation: the code is rearranged in several files and a message-passing interface using two-dimensional data decomposition of the horizontal domain has been implemented. POM has been applied extensively to the Mediterranean and the Strait of Gibraltar (e.g. Zavatarelli and Mellor, 1995; Ahumada and Cruzado, 2007; Jungclaus and Mellor, 2000; Drakopoulos and Lascaratos, 1999; Alhammoud et al., 2010; Sannino et al., 2002; Beckers et al., 2002). In an application to the Mediterranean, POM is set up with a true evaporation instead of a virtual salt flux. Evaporative water loss in the Mediterranean therefore drives a net flow through the Atlantic gateway which is necessary for a realistic representation of exchange.

Vertical mixing coefficients are calculated in the model with the Mellor and Yamada (1982) level 2.5 turbulence closure scheme. The pressure gradient scheme used is a fourth order scheme using the McCalpin method (Berntsen and Oey, 2010). The inverse Prandtl number, the ratio between horizontal mixing coefficients for diffusivity and viscosity (calculated with a Smagorinsky formulation), has been set to 0.2. This and other model parameters, chosen after an extensive sensitivity study, are listed in Table 1. The model parameter with the largest impact on model results proves to be the smoothing parameter of the Smolarkiewicz iterative upstream scheme.

The bathymetry used in this study (Fig. 1) derives from the 1 min resolution global surface (ETOPO1) provided by the National Geographical Data Center of the NOAA (Amante and Eakins, 2009). In the model, a curvilinear grid is used in the horizontal, similar to that of Zavatarelli and Mellor (1995). A curvilinear grid has the advantages that it allows for variable horizontal resolution and a high percentage of gridpoints in the basin, i.e. less gridpoints are needed compared to a rectangular grid. Before interpolation of the bathymetry to the horizontal grid (162 × 50 gridpoints), a Gaussian filter has been applied to remove short wavelength variations from the bathymetry. Furthermore, the parameter used to control the maximum slope between two adjacent gridcells is set to 0.15 in order to minimize pressure gradient errors and ensure model solution stability (Mellor et al., 1994). Horizontal grid resolution is highest near the Strait of Gibraltar and lowest in the eastern Mediterranean Basin. The minimum/maximum size of a grid cell in the "i" direction (Fig. 1) and "j" direction are respectively 11.7/62.9 and 10.7/69.6 km. The width of the Strait of Gibraltar is 12.9 km, equal to its smallest width at present-day. The orientation of the curvilinear coordinates (i and j) varies along the grid and deviates from the absolute longitudinal and latitudinal direction. For simplicity, the i and j directions along the curvilinear grid will be referred to as longitudinal and latitudinal,

CPD
10, 2979–3026, 2014

CC BY

respectively. Likewise, we will take "zonal" to mean "along the curvilinear i-coordinate". In the vertical direction, the grid comprises 40 sigma levels. Gridpoints have the highest density near the surface and bottom in order to resolve the thermocline and bottom currents. In order to optimize the time step, maximum depth in the Atlantic part of the model is set to 3000 m, in the Mediterranean to 4000 m. The maximum difference with the actual bathymetry is less than 100 m. In the current setup the model can be integrated for 100 yr in 28 h on 4 processors of an Intel Core i7-950 workstation running at 3.06 GHz with 12 GB memory.

Initial conditions for temperature and salinity derive from Levitus' World Ocean Atlas (Antonov et al., 1998). In the Atlantic part of the model, temperature and salinity are horizontally averaged before interpolation to sigma coordinates to avoid density contrasts near the western boundary of the grid, which is an open boundary, and provide water of constant temperature and salinity at each depth near the Strait of Gibraltar.

The surface forcing is idealized and constant in time, and resembles the forcing used in Alhammoud et al. (2010). The surface water flux is a constant evaporation of 0.5 m yr^{-1} over the whole model domain, a value close to present-day evaporation – precipitation – river input (Mariotti et al., 2002), but also suitable for the Late Miocene (Gladstone et al., 2007; Schneck et al., 2010). Sea surface temperatures are relaxed to a best fit for zonally and yearly averaged air temperatures from ECMWF data (Fig. 2 from Alhammoud et al., 2010). The relaxation time scale is 1 day; sensitivity experiments have shown that the relaxation time scale can be as long as 30 days before model results are significantly affected. Winds over the Mediterranean are highly variable throughout the year; a yearly averaged wind pattern is therefore unusable. Since wind stresses have been shown to affect only the strength of upper ocean circulation without changing the overal circulation pattern (Myers et al., 1998a; Meijer and Dijkstra, 2009), wind stresses have not been included.

The western boundary in the Atlantic part of the model domain is open. For the barotropic mode (2-D) a zero-gradient condition is applied to the free surface elevation, a clamped inflow condition is used for the depth-averaged velocity normal to the

CPD
10, 2979–3026, 2014

cc BY

open boundary, and a zero velocity is used for the boundary parallel velocity. For the baroclinic mode (3-D), a Sommerfeld radiation condition is applied to the velocity normal to the open boundary and a zero velocity is used, again, for the boundary parallel velocity. The inflow in the external mode compensates for the water volume lost by evaporation in the Mediterranean, keeping water volume constant. To avoid large temperature and/or salinity contrast between the inflow through the open boundary, which has a prescribed salinity and temperature equal to initial conditions, and the Atlantic part of the model, a relaxation back to initial Atlantic conditions is applied in the first 18 columns of the grid. The relaxation timescale in the surface layer varies from 3 months at the westernmost gridcell to 1 month at the easternmost gridcell of the relaxation area, and decreases exponentially in deeper layers.

3 Results and analysis

The results of a reference experiment, with idealized surface forcing and the sill depth of the Atlantic gateway set to the present-day depth of 300 m, will be compared with observations on the present-day Mediterranean. The experiments used to assess the role of sill depth only differ from the reference experiment in the sill depth and the bathymetry near the sill. The different experiments will be referred to as SD500 to SD5 according to their **S**ill **D**epth in meters. Each of the experiments has been run for 800 years. The time needed to reach steady state conditions in an experiment is inversely proportional to the depth of the sill. As a consequence, experiments with a sill depth below 100 m have not reached a steady state in 800 years. This will be pointed out where it affects the results.

3.1 Reference experiment

The temporal variation of basin-averaged temperature, salinity and a measure of kinetic energy, and strait transport is illustrated in Fig. 2 for the reference experiment (SD300).

Temperature, salinity and kinetic energy are averaged in the Mediterranean part of the model domain, i.e. east of the Strait of Gibraltar at -5.5° E. The average basinal velocity squared is used as a measure of the kinetic energy which, in turn, gives an indication of the intensity of flow in the basin. In the first 300 years of the reference experiment, salinity and temperature move towards their respective steady state values of 39.02 psu and 17.12°C. At the same time, inflow through the Strait of Gibraltar also stabilizes at 0.83 Sv (1 Sv = 10^6 m^3 s^{-1}). The difference between inflow and outflow, the net flow, is equal to the fresh water deficit in the Mediterranean, 0.04 Sv, from the start of the experiment. Salinity, temperature and strait transport all reach steady state values at the same time. This is the expected behaviour since salinity and temperature determine the density difference with the Atlantic, which, in turn, drives the exchange at Gibraltar. The kinetic energy measure reaches a value close to its steady state value within the first 100 years and slowly increases further towards a steady state, which is also reached at 300 yr.

At steady state a balance exists between the transport of heat and salt at the Strait of Gibraltar and the surface forcings in the Mediterranean, which is reflected by quasi-constant properties of the exchange. Velocity, temperature and salinity profiles from the Strait of Gibraltar are shown in Fig. 3. Relatively warm Atlantic water with a close to normal marine salinity flows eastwards through the Strait of Gibraltar in the upper layer, while more saline water flows westward at depth. The anti-estuarine circulation pattern observed in the present-day Strait of Gibraltar is thus reproduced. Moreover, the velocity profile is similar to observed velocity profiles at Camarinal Sill (e.g. Bryden et al., 1994; Tsimplis, 2000; Hopkins, 1999; Candela, 2001), velocity and salinity profiles of other model studies (Sannino et al., 2002; Xu et al., 2007), and theoretical velocity profiles (Hopkins, 1999). Small differences exist in the height of the interface and absolute velocities of inflow and outflow. These are mainly due to the idealized shape of the cross sectional area of the gateway in our model. The curves in Fig. 3 exhibit four features that are noteworthy: (1) the depth of the interface between the inflow and outflow is not exactly halfway but slightly deeper (165 m), (2) velocity changes gradu-

CPD
10, 2979–3026, 2014

CC BY

ally with depth, i.e. there is no sharp transition across the interface between inflow and outflow, (3) the maximum velocity in the outflow is higher than in the inflow because velocities are strongly reduced near the bottom, and (4) temperature and salinity gradually change with depth, indicating that mixing takes place between inflow and outflow in the strait. All four features are important when exchange in the experiments with different sill depths is compared to the exchange predicted by hydraulic control theory (Sect. 4.1).

Figure 4 illustrates the horizontal and vertical patterns of salinity and temperature in two horizontal slices at 10 m and 300 m and a vertical section crossing the whole domain from west to east. The inflowing Atlantic water starts to change its temperature and salinity in response to the surface forcing as soon as it enters the Mediterranean. At the surface, low saline Atlantic water can be traced along the southern coast into the eastern Mediterranean. The constant evaporation at the surface drives an increase in salinity towards the eastern basin, from 36.5 to 39 psu. Highest salinities are accordingly reached in the easternmost Mediterranean. Due to the strong surface temperature relaxation, surface temperatures are similar to the latitudinally decreasing air temperature in the larger part of the Mediterranean. Only the northern part of the western basin and the area directly east of the Sicily Strait deviate from this pattern. In both areas, advection of heat is faster than the surface forcing.

A difference in water characteristics does not only exist between the Atlantic and Mediterranean, a clear difference is also visible between western and eastern Mediterranean. The Sicily Strait restricts exchange between the basins. In combination with the fresh water deficit of the eastern Mediterranean, this drives an eastward surface flow and westward deep flow, i.e. an anti-estuarine circulation with respect to the western basin. The western basin has an average salinity of 38.3 psu, compared to 39.5 psu in the eastern basin. In spite of the significantly higher surface temperatures in the eastern basin, differences in basin-averaged temperature are relatively small (16.1 vs. 17.5 °C).

CPD
10, 2979–3026, 2014

R. P. M. Topper and P. Th. Meijer

CC BY

The circulation pattern evidenced by the salinity and temperature distribution in the Mediterranean is confirmed by the "zonal" overturning stream function which is calculated along the curvilinear coordinates (Fig. 5). A positive overturning cell, representing clockwise circulation in an W–E profile, extends from the Atlantic through the whole Mediterranean. The vertical extent and strength of the positive overturning cell is larger in the western than in the eastern Mediterranean. At depth a negative overturning cell is present in both basins with a larger vertical extent and strength in the eastern basin.

On the vertical temperature and salinity profiles, the area east of 25° E stands out due to its significantly higher salinity and temperature at depths up to 500 m. The zonal overturning stream function confirms that this is an area of downwelling. Following the approach from other studies (Dijkstra, 2008; Ezer and Mellor, 1997; Alhammoud et al., 2010), the rate of intermediate water formation can be derived from the stream function. In the area east of 25° E, the rate of intermediate water formation is 0.75 Sv. The tilted isotherm in the deep eastern basin is consistent with intermediate and deep water formation in the eastern part of the basin. The inclined isohalines in the upper 300 m of the western basin are not caused by vertical water movements but by the flow of more saline water from the eastern basin to the west.

For further analysis of the intermediate and deep water formation, Fig. 6 shows the distribution of the mixed layer depth. Deep water is formed where the mixed layer is anomalously deep, e.g. the northern part of the western basin where mixing occurs up to 800 m, and where the mixed layer depth equals the water depth, as in the Adriatic Sea, the Aegean Sea and the northeast corner of the Levantine Basin. Figure 6 shows the path of water particles that have been tracked for 30 days in the lowest sigma layer, i.e. the bottom currents. The idea of visualizing bottom velocities to track dense water currents is taken from Zavatarelli and Mellor (1995). Where dense water is formed in shallow areas, it flows downslope to the deep basin until it reaches a depth where its density equals that of the water at that depth. While dense water from the Adriatic clearly reaches large depths, dense water from the Aegean only reaches intermediate depths. In addition to deep water formation and dense water currents flowing into the

CPD
10, 2979–3026, 2014

R. P. M. Topper and P. Th. Meijer

CC BY

deep basin, Fig. 6 also shows the trajectories of dense water flowing from the eastern to the western basin and from the Mediterranean to the Atlantic. The northward deflection of both westward directed flows is due to the Coriolis effect.

3.1.1 Model results compared to present-day observations

Initial conditions in the model are based on recent observations of salinity and temperature (Levitus fields). Therefore, the difference between initial and steady state salinity and temperature is equal to the difference between modelled and observed values. Due to the simple constant surface forcings, we cannot expect to capture annual variability in circulation and deep water formation. A difference exists between the annual mean air temperature, used as surface forcing, and the observed annual mean sea surface temperature. This already indicates that water characteristics do not respond linearly to the surface forcing. Basin averaged temperatures are 3.4 °C higher than observed (17.12 vs. 13.71 °C). The bulk of this difference can be ascribed to significantly higher deep water temperatures. Temperature differences near the surface are comparatively small and, because only 10 % of the basinal volume is contained in the surface layer, do not significantly affect basin averages.

In the present-day Mediterranean, deep water formation is strongest during the winter months (e.g. Lascaratos et al., 1999). Hence, most deep water is formed when sea surface temperatures are below the annual average. The use of mean annual air temperatures in our model gives rise to deep water formation throughout the year and an associated overestimation of deep water temperatures. Basin averaged salinity, on the other hand, is close to the value from observations (39.0 vs. 38.6 psu). Annual variability of evaporation in the Mediterranean is small. The use of a constant evaporation rate is therefore a simplification of the surface forcing that does not significantly impact the basinal salinity. Furthermore, a model setup with a constant surface forcing provided a convenient starting point in unravelling a possible correlation between sill depth and the overturning.

CPD
10, 2979–3026, 2014

CC BY

The transport through the Strait of Gibraltar has been the subject of innumerable studies. Estimates have been based on observations, numerical modelling and hydraulic control theory. Given the uncertainty in the fresh water budget of the Mediterranean and the wide range of approaches, the volume transport at the Strait of Gibraltar has been estimated at 0.8–1.8 Sv, with most recent estimates at the lower end of this range (e.g. Astraldi et al., 1999; Tsimplis and Bryden, 2000). The inflow of 0.83 Sv in the reference experiment is thus within this range. In a model with annual variation in the surface forcing, the low deep water temperatures observed in the Mediterranean are reproduced (unpublished results). Compared to the results of the reference experiment, lower deep water temperatures will lead to a small increase of exchange due to the resultant larger density contrast with the Atlantic. However, for the objective of examining the role of strait depth, water exchange with the Atlantic is sufficiently reproduced.

Often, basin-scale circulation models with realistic and idealized atmospheric forcing have had difficulties reproducing deep water formation and, in particular, deep overturning in the western basin (e.g. Meijer et al., 2004; Meijer and Dijkstra, 2009). The reference experiment, set up with idealized forcing, is able to produce both. It should, however, be noted that the location of deep water formation in the model differs, especially near the Gulf of Lions, from locations inferred from observations.

In a series of sensitivity experiments, deep water formation has been compared in models with different latitudinal gradients in the air temperature. With a reduced latitudinal air temperature gradient, the mixed layer depth is still largest in the northern part of the western basin, the Adriatic and the Aegean Sea. However, rates of deep water formation and the strength of the deep overturning cell are lower while the formation of intermediate water in the eastern basin and the strength of the upper overturning cell in both basins are higher. These results are in agreement with Alhammoud et al. (2010) and Somot et al. (2006) who found that deep water formation is mainly controlled by the surface temperature forcing. These authors also found that intermediate

CPD
10, 2979–3026, 2014

cc BY

water formation is mainly controlled by evaporation. A series of sensitivity experiments with different rates of evaporation confirms this.

The strength of the surface overturning cell in the reference experiment is slightly larger than in most other high-resolution model studies (Meijer et al., 2004; Meijer and Dijkstra, 2009; Somot et al., 2006; Stratford et al., 2000; Adloff et al., 2011). The vertical and horizontal extent, however, is similar for both western and eastern basin. Also, the ratio between minimum and maximum zonal overturning is equal to other studies at ≈ 0.33. The results of a series of sensitivity experiments demonstrate that the degree of bathymetry smoothing, the maximum slope in the bathymetry and the smoothing parameter of the Smolarkiewicz scheme have a significant and predictable impact on the strength of circulation. In general, less smoothing, steeper slopes and a lower smoothing parameter result in a stronger overturning with more lateral variation. The bathymetry used here has relatively low maximum slopes and minimal smoothing while the smoothing parameter is relatively low.

The overall good agreement between observed and modelled strait transports, water characteristics and circulation, quantitatively as well as qualitatively, shows that the model setup of the reference experiment captures all important processes of the Mediterranean thermohaline circulation. Having validated the model setup of the reference experiment, we will describe in the next section the changes in Mediterranean water characteristics and circulation due to changes in the sill depth of the Atlantic connection.

3.2 The role of sill depth

The temporal variations of water characteristics and transport in two experiments with a shallow (50 m, SD50) and deep (500 m, SD500) gateway and the reference experiment can be compared in Fig. 2. The increase in basin-averaged temperature with run time in all three experiments is comparable in both magnitude and duration. A steady state is reached after 300 yr with a slightly lower value for SD500 (17.01 °C) and a higher value for SD50 (17.30 °C). The temporal variation of basin-averaged salini-

CPD
10, 2979–3026, 2014

cc BY

ties, on the other hand, is significantly different. SD500 reaches a steady state within 100 yr at 38.6 psu, SD50 does not reach a steady value within 800 yr. The average rate of salinity increase in SD50 is 8.9 psu kyr^{-1}. However, the rate drops slowly with time; in the first 100 yr it is 10.7 psu kyr^{-1}, in the last 100 yr "only" 6.8 psu kyr^{-1}. When the density difference between Atlantic and Mediterranean increases, inflow and outflow also increase. When a steady state is reached, the inflow volume multiplied with its salinity equals the outflow volume multiplied with its salinity. Before steady state more salt flows in than out, Mediterranean salinity increases, and, consequently, transport increases. The increasing transport reduces the difference between salt volume in inflow and outflow and, hence, the salinity rise slows down towards steady state. After 800 yr, all experiments with a sill depth ≥100 m (SD100–SD500) are in equilibrium, i.e. salinity and strait transport have reached a steady state.

The basin averages in Fig. 2 do not show where the differences in salinity and temperature arise between the different experiments. For this purpose, Fig. 7a shows the salinity averaged over depth and along the curvilinear j coordinate ("latitude") for every *i* coordinate. Due to the curvilinear grid, these depth-j slices are not exactly north-south. Latitude-depth-averaged temperature and density are calculated in a similar fashion (Fig. 7b and c). Also shown, in dashed lines, is the average temperature/salinity/density of the basin from the Gibraltar Strait up to each longitude. The temperature/salinity/density at the eastern end (36° E) is thus the basin averaged value.

Only where the bathymetry was modified to accomodate a different sill depth, i.e. between −6 to −2° E, does the shape of salinity curves differ between SD5–SD500. For a shallower sill depth the whole curve, apart from this westernmost segment, shifts to higher salinities. In each curve, salinity increases in two distinct steps at longitudes corresponding to the western basin – Tyrrhenian Sea connection (9° E) and the Sicily Strait (15° E) (Fig. 7c). Although salinities in each basin – western, Tyrrhenian and eastern basin – are higher at lower sill depths, the difference between them is nearly constant: ≈ 0.4 between the western basin and the Tyrrhenian, ≈ 0.8 between the Tyrrhenian and eastern basin. These steps are visible in this representation due to

CPD
10, 2979–3026, 2014

CC BY

fast changes in the water properties at the gateways, the cumulative average salinity increases more gradually.

Latitude-depth-averaged temperatures in Fig. 7b have a large spread near the gateway. Water depths near the gateway are shallower when the sill depth is lower, hence the influence of warm surface water on the average temperature in this area is larger and the temperature higher. In contrast to the salinity curves, the relative position of the temperature curves is not the same in all subbasins; in the western basin temperatures are relatively low in SD500–SD300 and SD20–SD5, in the eastern basin temperatures increase from SD500 to SD5. Given that surface forcing is constant, these differences must be caused by differences in the circulation which we will elaborate on below. Compared to the steps in the salinity curves, the changes in temperature occur in a broader range of longitudes. Due to the shallow depths near the connections between the basins, the warm surface layer becomes more important for the local average. Notwithstanding local differences, the trend in the basinal averages is towards higher temperatures at lower sill depths.

The density curves in Fig. 7c illustrate the combined effect of salinity and temperature. Because salinity is fairly stable in each subbasin, density changes in subbasins are caused by temperature differences. Because these temperature differences are mainly caused by different latitudinally averaged water depths, the density curve reflects the average water depth. Shallow low density areas are the connections between the subbasins, the Aegean Sea and the easternmost eastern basin.

The main features of the basinal circulation can be captured in the minimum and maximum strengths of the overturning cells and the depths where these occur in the western and eastern basin. These parameters are shown as a function of sill depth in Fig. 8. The upper cell is consistently deeper and stronger in the western than in the eastern basin (as visible in Fig. 6 for SD300). For the deep cell this pattern is reversed: it is consistently deeper and stronger in the eastern basin than in the western basin. In the experiments that have reached a steady state, i.e. SD100–SD500, strength and depth of all cells except the upper cell in the western basin are strikingly

CPD
10, 2979–3026, 2014

similar. In SD5–SD50, where a steady state has not yet been reached, the strength of the overturning cells changes significantly between 400 and 800 yr (light and dark symbols, respectively). Over this period, the strengths of the western deep cell and the eastern deep and upper cell in SD5–SD200 move towards the steady state value that is reached in SD100–SD500. This suggests that a similar overturning circulation will eventually be reached regardless of the sill depth. A difference not captured in Fig. 8, is the depth of the interface between the upper and deep overturning cells. Even though the depth of the minimum and maximum strength remains the same, the interface shifts to shallower depths when the upper overturning cell loses strength.

Compared to the overturning in steady state, deep overturning in the eastern basin is more vigorous before a steady state is reached. In the western basin deep overturning is weaker before a steady state, as are the surface cells in the western and eastern basin. Towards a steady state, deep water formation in the eastern basin slows down when the vertical density gradient in the basin stabilizes. At the same time, intermediate water formation in both basins and deep water formation in the western basin pick up when vertical temperature differences decrease.

The only cell that stabilizes at a different strength depending on sill depth, is the upper cell in the western basin. The increase in overturning strength from SD100 to SD500 (+0.84 Sv) is similar to the increase in exchange with the Atlantic (+0.91 Sv, Fig. 9). From this similarity it can be inferred that the upper overturning cell in the western basin is mainly controlled by the exchange with the Atlantic. The temperatures in the western basin are consistent with this: temperatures are lower, i.e. closer to Atlantic values, when the exchange with the Atlantic is larger (SD100 to SD500). SD5–SD20 deviate from this trend (Fig. 7b). However, not being in steady state, the deep water temperature in the western basin is still rising after 800 yr in these experiments.

The temperature in the eastern basin is only affected by the magnitude of the Atlantic-derived inflow in the surface layer near the Strait of Sicily. Therefore, a reduced Atlantic inflow cannot explain the small temperature increase from SD500 to SD100 in the eastern basin (Fig. 7b). This temperature increase is most pronounced below

CPD
10, 2979–3026, 2014

Discussion Paper | Discussion Paper | Discussion Paper | Discussion Paper |
Title Page
Abstract | Introduction
Conclusions | References
Tables | Figures
◀| |▶
◀ ▶
Back | Close
Full Screen / Esc
Printer-friendly Version
Interactive Discussion

CC BY

250 m and associated with a small change in overturning circulation. The upper and lower cell in the eastern basin are minimally stronger in SD100 compared to SD500. In the reference experiment, deep water was formed where sea surface temperatures were low, and intermediate water where maximum salinities were reached near Cyprus. At higher salinities, the change in density caused by cooling of surface water is comparatively smaller. As a consequence, lateral and vertical density differences at the surface are smaller and mixed layer depth increases significantly throughout the eastern basin. This drives a stronger intermediate water formation and slightly enhances the strength of the upper overturning cell. Noteworthy is the instatement of a new branch of intermediate water formation in the northern Ionian Basin in lower sill depth experiments. This area receives less relatively low saline water from the western basin at lower Atlantic sill depths due to a lower density difference between the basins. Consequently, water becomes dense enough to sink in this area. Compared to the dense water formation sites in the Adriatic and Aegean, surface water is warmer in the Ionian Basin. Due to the reduced vertical density gradient at lower sill depths, dense water formed in the Adriatic flows downslope to greater depths, thereby enhancing the strength of the deep overturning cell. In summary, lower density gradients at lower sill depth enhance upper and deep overturning circulation in the eastern basin which leads to the small increase in intermediate and deep water temperatures observed in Fig. 7b.

3.2.1 Strait transport

The magnitude of modelled strait transport as a function of sill depth is illustrated in Fig. 9 (red plusses). Down to a sill depth of 20 m, inflow decreases steadily towards the value of net flow (blue plusses) which is essentially constant in all runs. Inflow is almost linearly proportional to sill depth; only towards higher sill depths does the increase in inflow flatten slightly. Outflow is not shown because it shows the same trend as the inflow (outflow being inflow minus net flow).

Even though the Atlantic–Mediterranean exchange appears to be a simple two-way flow from Fig. 9, velocity, salinity, temperature and density profiles in the gateway show

CPD
10, 2979–3026, 2014

CC BY

that this is not true (Fig. 10). Velocity (Fig. 10a) is positive in the top layer and decreases gradually towards the interface between inflow and outflow, at a depth lower than half the sill depth, and decreases again towards the bottom due to bottom friction. Salinity (Fig. 10b) in the top layer is near constant at all sill depths, being supplied with Atlantic water with relatively constant salinity. The lower layer becomes increasingly more saline towards lower sill depths in accordance with the average basinal salinity. Temperatures (Fig. 10d) decrease in the top layer from the surface to the interface depth, and increase again towards the bottom. The high temperatures at the surface are caused by the heat flux at the surface. In the Atlantic, temperatures drop significantly with depth (Fig. 4). In the surface inflow this results in a lower temperature near the interface depth at higher sill depths. In the Mediterranean, temperatures decrease less with depth. Therefore, temperatures in the outflow move back to higher values away from the interface. The gradual change of velocity, temperature and salinity between inflow and outflow indicates mixing between the two layers. The combined effect of salinity and temperature is expressed in the density profiles (Fig. 10). Towards lower sill depths the density difference between the Atlantic surface flow and Mediterranean outflow becomes larger. i.e. density changes faster over a shorter vertical distance.

In SD5 and SD10, inflow is constant and equal to the net flow, i.e. there is no outflow. Although outflow is blocked in these two experiments, neither experiment has reached a steady state yet. Salinity rises constantly at 11.6 psu kyr^{-1} as long as outflow is blocked because all salt that enters the Mediterranean through inflow (4.3×10^{13} kg yr^{-1}) is retained in the Mediterranean. In SD20 and SD50, like SD5 and SD10 not yet in steady state, the ongoing salinity rise in the Mediterranean is accompanied by a steady increase in the outflow and, hence, inflow. It is possible that the increasing density difference between Mediterranean and Atlantic in SD10 and SD5 will eventually incite two-way flow. However, the anticipated salinities for the steady states in these experiments are >100 psu, which will take at least another 5000 yr to be reached. Therefore, due to the additional model run time required, reaching steady states in SD5 and SD10 is infeasible in the current model setup. Moreover, the equa-

CC BY

tion of state – which relates temperature, salinity and pressure to density – is only valid up to 42 psu. At higher salinities, a linear extrapolation is used to calculate the density increase due to salinity. This will give an increasingly larger error in the density determination towards higher salinities. Also, the viscosity of water will change significantly at such high salinities, a process not included in the model.

In summary, exchange between the Mediterranean and Atlantic is proportional to the sill depth until at 10 m sill depth outflow is blocked and only inflow remains. The interface between inflow and outflow is consistently deeper than half the sill depth. The highest velocities are reached in the saline, warm Mediterranean outflow which is overlain by a less saline, colder Atlantic inflow.

4 Discussion

4.1 Hydraulic control

A comparison of exchange in the model and that predicted by hydraulic control theory is called for since hydraulic control theory has been extensively used to describe the Atlantic–Mediterranean exchange. Hydraulic control theory can be used to calculate the flow through a narrow strait if the geometry and density difference along the strait are known. A recent overview of the basic principles underlying hydraulic control theory and an application to the Mediterranean can be found in Meijer (2012). Differences between exchange calculated with hydraulic control theory and that from the model are to be expected due to the more complex physics in the model. For comparison with the modelled exchange, an expression for hydraulic control for a strait with a rectangular cross section and zero net flow is used (Farmer and Armi, 1986; Bryden and Kinder, 1991):

$$Q_\mathrm{A} = Q_\mathrm{M} = 0.208 \cdot \sqrt{g'H}HW \quad (1)$$

Discussion Paper | Discussion Paper | Discussion Paper | Discussion Paper |

CPD

10, 2979–3026, 2014

Mediterranean response to gateway restriction

R. P. M. Topper and P. Th. Meijer

Title Page
Abstract Introduction
Conclusions References
Tables Figures
◀I ▶I
◀ ▶
Back Close
Full Screen / Esc
Printer-friendly Version
Interactive Discussion

cc BY

where Q_A, is the inflow from the Atlantic which is equal to the outflow from the Mediterranean, Q_M; H is the sill depth, W the strait width, and the reduced gravity, g', is defined by

$$g' = g\left(\rho_M - \rho_A\right)/\rho_M \quad (2)$$

where g is the gravitational acceleration, ρ_M, Mediterranean outflow water density and ρ_A Atlantic water density.

Besides the modelled strait transport, Fig. 9 also shows the inflow calculated with Eq. (1) for a strait with the same dimensions (width and depth) as in the model; Atlantic and Mediterranean basin-averaged densities are used as ρ_A and ρ_M respectively. Compared to the strait transport predicted by hydraulic control, the modelled transports are consistently lower. The absolute difference as well as the ratio between inflow predicted by hydraulic control and inflow from the model decrease towards lower sill depths, i.e. modelled transport is closer to that predicted by hydraulic control in shallower gateways.

In hydraulic control theory, the velocity and density profiles at the gateway are envisaged to be a step function with a constant positive velocity and low density in the upper layer and a constant negative velocity and high density in the bottom layer. In contrast, profiles derived from the model (Fig. 10) show a gradual change in water properties near the interface between inflow and outflow. It must be noted, however, that density and salinity profiles at lower sill depths are closer to a step function than those at larger sill depths; a larger change in salinity/density occurs in a smaller depth interval. This may partly explain why hydraulic control theory better matches modelled transports at lower sill depths.

When transport is calculated by inserting the average density of inflow and outflow in Eq. (1), instead of averages of Atlantic and Mediterranean basins, it is closer to modelled values at low sill depths and further from modelled values at large sill depths. The density difference between inflow and outflow is larger than between the basin averages at large sill depths, while it is smaller for lower sill depths. At sill depths > 100 m,

CPD
10, 2979–3026, 2014

CC BY

mixing between the inflow and outflow reduces the temperature of the outflow, which is already more saline than the inflow, and lowers the density. Hence, the density contrast between inflow and outflow is increased compared to the difference between the basin averages. Consequently, the inflow predicted by hydraulic control with the densities in the gateway is higher than that with basin average densities. At sill depths < 100 m, the density difference between the inflow and outflow is smaller than the difference between basin averages because the largest difference in temperature between the basins occurs at greater depths than those involved in the exchange. Accordingly, the inflow predicted by hydraulic control with densities in the gateway is lower than that from basin averaged densities and closer to modelled transports.

Regardless of the densities used, exchange calculated with hydraulic control theory is always larger than modelled transport. The aforementioned vertical mixing between inflow and outflow is one obvious cause of the difference. Another important factor is friction; at the bottom it slows down the outflow and friction between the inflow and outflow slows down both. Coriolis force does not play a role here due to the narrow width of the gateway.

In summary, transport at lower sill depths is closer to that predicted by hydraulic exchange theory than at large sill depths because mixing between inflow and outflow is not as effective in reducing the difference between them. Furthermore, using basin averaged density differences for calculation of the exchange with hydraulic control gives an overestimation of the exchange because water characteristics at the depths involved in the exchange are not representative of the whole basin.

4.2 The role of sill depth

In experiments with sill depths in the range of 500–5 m, basin-averaged salinities and temperatures are consistently higher at lower sill depths. Spatial differences, e.g. between the western and eastern basin, are largely independent of sill depth. The upper overturning cell in the western basin is controlled by the exchange with the Atlantic and is weaker at lower sill depths. The upper overturning cell in the eastern basin and

CPD
10, 2979–3026, 2014

cc BY

the deep overturning cells in both basins, however, are practically constant in depth and strength at all sill depths as soon as a steady state has been reached. Dense water formation is more salinity-driven when basin averaged salinities are higher; at high salinities surface cooling causes a smaller percentual increase of density than at low salinities. However, overall, the locations and rate of dense water formation change little.

The influence of sill depth on circulation and water characteristics found in this study is, mainly due to differences in model setup, different from that found by Alhammoud et al. (2010) (AMD10). In AMD10, a highly idealized representation of the Mediterranean was used, which consists of a single large basin with a depth of 1500 m gradually shallowing towards the margins. In accordance with our findings for the western basin they found a steadily increasing inflow and stronger upper zonal overturning cell in experiments with increasingly larger sill depths. Their deep overturning cell, however, almost disappears at large sill depths whereas it is here found to be constant in strength regardless of sill depth. The shift of the interface between upper and deep overturning cells in their experiments does resemble the shift found here. Because their basin extends to only 1500 m, the deep overturning cell is suppressed by stronger surface cells when these extend to greater depths, while it persists below 1500 m in our experiments. As in our experiments, deep water circulation, although strongly reduced, never entirely stopped in the experiments of AMD10.

The low resolution used in AMD10 resulted in a 222 km wide Strait of Gibraltar. Due to this width, exchange with the Atlantic was found to be consistent with rotational control on the flow instead of hydraulic control. The width of the Strait of Gibraltar in our model (13 km) is well below the Rossby radius and, hence, rules out rotational control. The larger strait transports in AMD10 kept Mediterranean salinities closer to Atlantic values, but the overall trend towards higher salinities at lower sill depths is consistent with our findings.

CPD
10, 2979–3026, 2014

R. P. M. Topper and P. Th. Meijer

CC BY

4.3 The interpretation of the Late Miocene sedimentary record

As argued in the introduction, we expect that the change in circulation and water properties due to variation in sill depth that we calculated for a basin with the shape of the present Mediterranean forms a starting point for understanding the past as well. In this section we relate our findings to the Late Miocene sedimentary record.

Stable isotopes and faunal changes in the pre-MSC interval of the Late Miocene, suggest that in an interval with increasing salinity, the average deep water oxygenation decreased steadily (Kouwenhoven and van der Zwaan, 2006). As already noted by Kouwenhoven and van der Zwaan (2006) and Krijgsman et al. (2000), the occurrence of sapropels in this interval indicates precessional variation of the oxygenation of Mediterranean deep water on top of the long term trend. The estimated depth of the marginal basins in which the Monte del Casino, Metochia, Faneromeni and Gibliscemi sections accumulated is 300–1200 m. In these basins the decreasing oxygenation and sapropelitic sedimentation are observed. All are located in the eastern Mediterranean basin in which, in our model, the upper overturning cell is less than 500 m deep. If rates of deep water formation and the strength of deep overturning are lower at lower sill depths, oxygen conditions in the deep water layer would decrease concomitant with a decreasing gateway depth. Model results, however, do not show a significant change in either deep water formation or deep overturning in the eastern basin.

In the western basin, depths up to 1200 m are in the upper overturning cell in SD500–SD100. Oxygenation of the marginal basins in this setting would not be by deep water formation, but by intermediate water formation in the upper overturning cell. The simultaneous decrease of exchange with the Atlantic and strength of the upper overturning cell in the western basin towards lower sill depths leads to a longer residence time of the water in the upper cell of the western basin. Consequently, water in the marginal basins will be replenished slower with oxygenated water from the surface. Therefore, model results from the western basin could explain the suggested correlation between sill depth and oxygenation. Because AMD10 represents the Mediterranean with only

Discussion Paper | Discussion Paper | Discussion Paper | Discussion Paper |

CPD
10, 2979–3026, 2014

one basin, their correlation between observations and model results is similar to what is here suggested for the western basin.

Model results thus seem to contradict the notion that restriction of the Atlantic–Mediterranean gateway induces lower oxygenation of deep water in the eastern basin. A lower oxygenation may, however, be inferred for the upper overturning cell in the western basin. Due to the relatively shallow connection between the western and eastern basin, only the western overturning is affected by sill depth in a way that seems consistent with the data. A possible cause of the discrepancy between model results and observations is the present-day bathymetry used in the model. If the connection between both basins was deeper in the Late Miocene, the upper overturning cell could have extended further and deeper into the eastern basin. Without the Sicily Strait, model results are expected to be similar to those in AMD10 who indeed had a single surface overturning cell in the whole Mediterranean.

At present day, deep water formation is mainly driven by cooling of surface water during the winter. In the model, deep water formation is likewise driven by surface cooling at northern latitudes. Despite the fact that deep water formation is continuous, occurring at the same rate throughout the year, the forcing that drives deep water formation is the same. We, therefore, argue that deep water formation is sufficiently represented in our setup to reproduce possible changes in deep water oxygenation that may occur in a less idealized case.

Another simplification in the surface forcing, on the other hand, may influence the correlation of model results and observations: the inclusion of river discharge in a uniform surface flux equal to E-P-R. Increased river discharge during precession minima is generally accepted to be an important factor in the establishment of low-oxygen conditions during sapropel formation. River discharge is thought to form a fresh-water-lid at the surface, hindering deep water formation by reducing surface layer densities. Due to mixing with more saline water and evaporative concentration, water originating from rivers will lose its fresh water signature when it moves away from the outlet. If the receiving basin is at higher salinity, the density difference between river water and the

CPD
10, 2979–3026, 2014

R. P. M. Topper and P. Th. Meijer

CC BY

basin is larger and stratification will be stronger. Although depending on the volume and location of river input, basin circulation, evaporation – precipitation, and the rate of mixing with surrounding water, we can assume that stratification due to river discharge is stronger when the basin-averaged salinity is higher. Hence, deep water formation may be more effectively reduced at lower sill depth. If a river drains into a marginal basin with restricted exchange with the deep basin, stratification is presumably more severe and deep water oxygenation even stronger reduced.

A spatially heterogeneous distribution of precipitation may have the same effect as river discharge. Precipitation, however, does not give a continuous fresh water input at the same location like river input. Hence, its influence with respect to river discharge is expected to be lower.

4.4 Blocked outflow

Notwithstanding the fact that SD10 and SD5 are not yet in steady state, it is the first time that a blocked outflow has been observed in an ocean circulation model in this context. From hydraulic control theory, one layer flow is predicted to occur only when the sill depth is a few meters for a gateway with a width of 13 km (Meijer, 2012). If bottom friction is taken into account, this depth is expected to be somewhat higher. Because the density difference between the Atlantic and Mediterranean is still rising at the time model results are shown for, it may be that outflow will commence if the experiment is ran to steady state.

Our model results suggest that if a sill depth of ≈ 10 m existed during the MSC, either due to a global sea level drop or local uplift due to flexure or tectonics, the salinity rise in the Mediterranean would be maximal. Consequently, the salt gain of the Mediterranean is highest in this scenario, allowing for the fast accumulation of evaporites. During blocked outflow 15 km^3 halite is transported to the Mediterranean every year. At this rate it would take 33–133 kyr to form the 0.5–2 million km^3 of halite observed on seismics (Ryan, 2008). Halite formation in the deep Mediterranean basins took place during an 60 kyr interval which encompasses two glacials: 5.61–5.55 Ma with glacials TG12 and TG14. The growth of icecaps on the poles during this interval would reduce global sea level, lowering the relative sill depth. Furthermore, glacials are characterized by a relatively high fresh water deficit in the Mediterranean due to reduced river discharge and precipitation. In this situation, salinity rise and salt gain will be even higher than found in our model. During blocked outflow inflow can thus bring in the observed volume of salt in the 60 kyr MSC interval. The blocked-outflow scenario is therefore plausible. To examine whether blocked-outflow endures at higher density contrasts a model should be set up to represent only the Strait of Gibraltar, or another gateway thought to be open during the Messinian. This, however, is impossible with the current model because the equation of state implemented in POM is not valid at salinities larger than 42 psu and anticipated viscosity changes at high salinities cannot be dealt with.

5 Conclusions

In this study, a parallel version of POM (sbPOM) has been used to examine changes in Mediterranean circulation and water characteristics due to restriction of the Atlantic connection. Model results have implications for the interpretation of the Late Miocene sedimentary record in the Mediterranean. Compared to earlier models of the (Miocene) Mediterranean, the use of a curvilinear grid and parallel code allows for the use of a higher resolution and more realistic bathymetry even in long model runs (800 yr). A comparison of the results from our model with observations of the present-day shows that, despite an idealized and constant surface forcing, Mediterranean circulation and water properties are generally well reproduced.

The model setup presented in this study would seem to provide a valuable basis and reference for examination of additional aspects of Mediterranean palaeoconfigurations. This may relate to other aspects of the Miocene evolution, for example, but our setup is also applicable to the Last Glacial Maximum when lower sea level was responsible for a reduction in sill depth.

CPD
10, 2979–3026, 2014

CC BY

The main results and implications for the Late Miocene Mediterranean are the following:

- Basin-averaged salinity, temperature and density increase when the sill is shallower. However, spatial distribution and inter-basinal differences in water properties in the Mediterranean are largely unaffected by sill depth.
- The strength of the upper overturning cell in the western Mediterranean is proportional to the magnitude of water exchange with the Atlantic. Overturning in the eastern basin is not significantly affected by the depth of the sill.
- Temperature-driven dense water formation operates regardless of the basin-averaged salinity. At lower sill depths, the higher salinity in the Mediterranean results in a stronger salinity-driven dense water formation in the eastern basin.
- Modelled strait transport is always smaller than that predicted by hydraulic control theory. This difference is due to friction, vertical mixing and a difference between basin-averaged density and the density of the water involved in the exchange with the Atlantic.
- Outflow is blocked in (at least the first 800 yr of) experiments with sill depths ≤ 10 m. Future work is needed to establish whether blocked-outflow is a viable scenario for the interval with halite deposition in the Messinian Salinity Crisis.
- With the present-day bathymetry, restriction of the Atlantic–Mediterranean connection does not significantly alter Mediterranean deep water circulation and refreshening. Hence, model results do not affirm the hypothesis that deep water ventilation decreases at lower sill depths.

Acknowledgements. The authors would like to thank Rinus Wortel for valuable input on drafts of this article. RPMT is supported by the Netherlands Research Center for Integrated Solid Earth Science. Computational resources for this work were also provided by ISES (ISES 3.2.5 High End Scientific Computation Resources). Figures in this paper were created using GMT version 4.5.1 (Wessel and Smith, 1991).

CC BY

References

Adloff, F., Mikolajewicz, U., Kučera, M., Grimm, R., Maier-Reimer, E., Schmiedl, G., and Emeis, K.-C.: Corrigendum to "Upper ocean climate of the Eastern Mediterranean Sea during the Holocene Insolation Maximum – a model study" published in Clim. Past, 7, 1103–1122, 2011, Clim. Past, 7, 1149–1168, doi:10.5194/cp-7-1149-2011, 2011. 2994

Ahumada, M. A. and Cruzado, A.: Modeling of the circulation in the Northwestern Mediterranean Sea with the Princeton Ocean Model, Ocean Sci., 3, 77–89, doi:10.5194/os-3-77-2007, 2007. 2985

Alhammoud, B., Meijer, P. Th., and Dijkstra, H. A.: Sensitivity of Mediterranean thermohaline circulation to gateway depth: a model investigation, Paleoceanography, 25, PA2220, doi:10.1029/2009PA001823, 2010. 2985, 2987, 2991, 2993, 3003

Amante, C. and Eakins, B. W.: ETOPO1 1 arc-minute global relief model: procedures, data sources and analysis, NOAA Technical Memorandum NESDIS NGDC-24, 19 pp., 2009. 2986

Antonov, J. I., Levitus, S., Boyer, T. P., Conkright, M. E., O'Brien, C., and Stephens, T. D.: World Ocean Atlas Data 1998, NOAA Atlas NESDIS, vol. 27, 166, 1998. 2987

Astraldi, M., Balopoulos, S., Candela, J., Font, J., Gacic, M., Gasparini, G. P., Manca, B., Theocharis, A., and Tintoré, J.: The role of straits and channels in understanding the characteristics of Mediterranean circulation, Prog. Oceanogr., 44, 65–108, 1999. 2981, 2984, 2993

Beckers, J.-M., Rixen, M., Brasseur, P., Brankart, J.-M., Elmoussaoui, A., Crépon, M., Herbaut, C.., Martel, F., Van den Berghe, F., Mortier, L., Lascaratos, A., Drakopoulos, P., Korres, G., Nittis, K., Pinardi, N., Masetti, E., Castellari, S., Carini, P., Tintore, J., Alvarez, A., Monserrat, S., Parrilla, D., Vautard, R., and Speich, S.: Model intercomparison in the Mediterranean: MEDMEX simulations of the seasonal cycle, J. Marine Syst., 33, 215–251, 2002. 2986

Benson, R. H., Bied, K. R.-E., and Bonaduce, G.: An important current reversal (influx) in the Rifian corridor (Morocco) at the Tortonian-Messinian boundary: the end of the Tethys ocean, Paleoceanography, 6, 164–192, 1991. 2983

Berntsen, J. and Oey, L.-Y.: Estimation of the internal pressure gradient in σ-coordinate ocean models: comparison of second-, fourth-, and sixth-order schemes, Ocean Dynam., 60, 317–330, 2010. 2986

CPD
10, 2979–3026, 2014

Mediterranean response to gateway restriction

R. P. M. Topper and P. Th. Meijer

cc BY

Bertini, A.: The Northern Apennines palynological record as a contribute for the reconstruction of the Messinian palaeoenvironments, Sediment. Geol., 188–189, 235–258, 2006. 2982

Betzler, C., Braga, J. C., Martín, J. M., Sánchez-Almazo, I. M., and Lindhorst, S.: Closure of a seaway: stratigraphic record and facies (Guadix Basin, Southern Spain), Int. J. Earth Sci., 95, 903–910, 2006. 2983

Blumberg, A. F. and Mellor, G. L.: A description of a three-dimensional coastal ocean circulation model, Coast. Est. S., 4, 1–16, 1987. 2985

Bryden, H. L. and Kinder, T. H.: Steady two-layer exchange through the Strait of Gibraltar, Deep-Sea Res., 38, S445–S463, 1991. 2981, 3000

Bryden, H. L. and Stommel, H. M.: Limiting processes that determine basic features of the circulation in the Mediterranean Sea, Oceanol. Acta, 7, 289–296, 1984. 2984

Bryden, H. L., Candela, J., and Kinder, T. H.: Exchange through the Strait of Gibraltar, Prog. Oceanogr., 33, 201–248, 1994. 2984, 2989

Candela, J.: The Gibraltar Strait and its role in the dynamics of the Mediterranean Sea, Dynam. Atmos. Oceans, 15, 267–299, 1991. 2984

Candela, J.: Mediterranean Water and Global Circulation, International Geophysics, vol. 77, chap. 5.7, Academic Press, San Diego, 419–429, 2001. 2989

Cramp, A. and O'Sullivan, G.: Neogene sapropels in the Mediterranean: a review, Mar. Geol., 153, 11–28, 1999. 2981

de la Vara, A., Meijer, P. Th., and Wortel, M. J. R.: Model study of the circulation in the Miocene Mediterranean Sea and Paratethys: closure of the Indian gateway, submitted, 2014. 2981

Dercourt, J., Gaetani, M., Vrielynck, B., Barrier, E., Biju-Duval, B., Brunet, M. F., Cadet, J. P., Crasquin, S., and Sandulescu, M. (eds.): Peri-Tethys Palaeogeographical Atlas, CCGM/CGMW, 2000. 2981

Dijkstra, H. A.: Scaling of the Atlantic meridional overturning circulation in a global ocean model, Tellus A, 60, 749–760, 2008. 2991

Drakopoulos, P. G. and Lascaratos, A.: Modelling the Mediterranean Sea: climatological forcing, J. Marine Syst., 20, 157–173, 1999. 2985

Duggen, S., Hoernle, K., van den Bogaard, P., Rüpke, L., and Phipps Morgan, J.: Deep roots of the Messinian salinity crisis, Nature, 422, 602–606, 2003. 2983

Ezer, T. and Mellor, G. L.: Simulations of the Atlantic Ocean with a free surface sigma coordinate ocean model, J. Geophys. Res.-Oceans, 102, 15647–15657, 1997. 2991

CC BY

Farmer, D. M. and Armi, L.: Maximal two-layer exchange over a sill and through the combination of a sill and contraction with barotropic flow, J. Fluid Mech., 164, 53–76, 1986. 3000
Fauquette, S., Suc, J.-P., Bertini, A., Popescu, S.-M., Warny, S., Bachiri Taoufiq, N., Perez Villa, M.-J., Chikhi, H., Feddi, N., Subally, D., Clauzon, G., and Ferrier, J.: How much did climate force the Messinian salinity crisis? Quantified climatic conditions from pollen records in the Mediterranean region, Palaeogeogr. Palaeocl., 238, 281–301, 2006. 2982
Gennari, R., Manzi, V., Angeletti, L., Bertini, A., Biffi, U., Ceregato, A., Costanza, C., Gliozzi, E., Lugli, S., Menichetti, E., Rosso, A., Roveri, M., and Taviani, M.: A shallow water record of the onset of the Messinian salinity crisis in the Adriatic foredeep (Legnagnone section, Northern Apennines), Palaeogeogr. Palaeocl., 286, 145–164, 2013. 2982
Gladstone, R., Flecker, R., Valdes, P., Lunt, D., and Markwick, P.: The Mediterranean hydrologic budget from a Late Miocene global climate simulation, Palaeogeogr. Palaeocl., 251, 254–267, 2007. 2987
Govers, R.: Choking the Mediterranean to dehydration: the Messinian salinity crisis, Geology, 37, 167–170, 2009. 2983
Hilgen, F. J., Krijgsman, W., Langereis, C. G., Lourens, L. J., Santarelli, A., and Zachariasse, W. J.: Extending the astronomical (polarity) time scale into the Miocene, Earth Planet. Sc. Lett., 136, 495–510, 1995. 2981
Hopkins, T. S.: The thermohaline forcing of the Gibraltar exchange, J. Marine Syst., 20, 1–31, 1999. 2984, 2989
Hüsing, S. K., Oms, O., Agustí, J., Garcés, M., Kouwenhoven, T. J., Krijgsman, W., and Zachariasse, W.-J.: On the late Miocene closure of the Mediterranean–Atlantic gateway through the Guadix Basin (southern Spain), Palaeogeogr. Palaeocl., 291, 167–179, 2010. 2983
Iovino, D., Straneo, F., and Spall, M. A.: On the effect of a sill on dense water formation in a marginal sea, J. Mar. Res., 66, 325–345, 2008. 2984
Ivanovic, R. F., Flecker, R., Gutjahr, M., and Valdes, P. J.: First Nd isotope record of Mediterranean–Atlantic water exchange through the Moroccan Rifian Corridor during the Messinian Salinity Crisis, Earth Planet. Sc. Lett., 368, 163–174, 2013. 2983
Jordi, A. and Wang, D.-P.: sbPOM: A parallel implementation of Princenton Ocean Model, Environ. Modell. Softw., 38, 59–61, 2012. 2985
Jungclaus, J. H. and Mellor, G. L.: A three-dimensional model study of the Mediterranean outflow, J. Marine Syst., 24, 41–66, 2000. 2985

CPD
10, 2979–3026, 2014

Mediterranean response to gateway restriction

R. P. M. Topper and P. Th. Meijer

Title Page
Abstract Introduction
Conclusions References
Tables Figures
◀ ▶
Back Close
Full Screen / Esc
Printer-friendly Version
Interactive Discussion

Karami, M. P., De Leeuw, A., Krijgsman, W., Meijer, P. Th., and Wortel, M. J. R.: The role of gateways in the evolution of temperature and salinity of semi-enclosed basins: an oceanic box model for the Miocene Mediterranean Sea and Paratethys, Global Planet. Change, 79, 73–88, 2011. 2981

Kouwenhoven, T. J. and van der Zwaan, G. J.: A reconstruction of late Miocene Mediterranean circulation patterns using benthic foraminifera, Palaeogeogr. Palaeocl., 238, 373–385, 2006. 2982, 3004

Kouwenhoven, T. J., Hilgen, F. J., and van der Zwaan, G. J.: Late Tortonian–early Messinian stepwise disruption of the Mediterranean–Atlantic connections: constraints from benthic foraminiferal and geochemical data, Palaeogeogr. Palaeocl., 198, 303–319, 2003. 2982

Krijgsman, W. and Meijer, P. Th.: Depositional environments of the Mediterranenan "Lower Evaporites" of the Messinian salinity crisis: constraints from quantitative analysis, Mar. Geol., 253, 73–81, 2008. 2982, 2983

Krijgsman, W., Hilgen, F. J., Raffi, I., Sierro, F. J., and Wilson, D. S.: Chronology, causes and progression of the Messinian Salinity Crisis, Nature, 400, 652–655, 1999a. 2982

Krijgsman, W., Langereis, C. G., Zachariasse, W. J., Boccaletti, M., Moratti, G., Gelati, R., Iaccarino, S., Papani, G., and Villa, G.: Late Neogene evolution of the Taza-Guercif Basin (Rifian Corridor, Morocco) and implications for the Messinian salinity crisis, Mar. Geol., 153, 147–160, 1999b. 2983

Krijgsman, W., Garcés, M., Agustí, J., Raffi, I., Taberner, C., and Zachariasse, W. J.: The "Tortonian salinity crisis" of the eastern Betics (Spain), Earth Planet. Sc. Lett., 181, 497–511, 2000. 3004

Lascaratos, A., Roether, W., Nittis, K., and Klein, B.: Recent changes in deep water formation and spreading in the eastern Mediterranean Sea: a review, Prog. Oceanogr., 44, 5–36, 1999. 2992

Mariotti, A., Struglia, M. V., Zeng, N., and Lau, K.-M.: The hydrological cycle in the Mediterranean region and implications for the water budget of the Mediterranean Sea, J. Climate, 15, 1674–1690, 2002. 2987

Martín, J. M., Braga, J. C., Aguirre, J., and Puga-Bernabéu, A.: History and evolution of the North-Betic Strait (Prebetic Zone, Betic Cordillera): a narrow, early Tortonian, tidal-dominated, Atlantic–Mediterranean marine passage, Sediment. Geol., 216, 80–90, 2009. 2983

CPD
10, 2979–3026, 2014

R. P. M. Topper and P. Th. Meijer

CC BY

Meijer, P. Th.: A box model of the blocked-outflow scenario for the Messinian Salinity Crisis, Earth Planet. Sc. Lett., 248, 486–494, 2006. 2982

Meijer, P. Th.: Hydraulic theory of sea straits applied to the onset of the Messinian Salinity Crisis, Mar. Geol., 326–328, 131–139, 2012. 2982, 3000, 3006

Meijer, P. Th. and Dijkstra, H. A.: The response of Mediterranean thermohaline circulation to climate change: a minimal model, Clim. Past, 5, 713–720, doi:10.5194/cp-5-713-2009, 2009. 2984, 2987, 2993, 2994

Meijer, P. Th. and Krijgsman, W.: A quantitative analysis of the desiccation and re-filling of the Mediterranean during the Messinian Salinity Crisis, Earth Planet. Sc. Lett., 240, 510–520, 2005. 2981

Meijer, P. Th. and Tuenter, E.: The effect of precession-induced changes in the Mediterranean freshwater budget on circulation at shallow and intermediate depth, J. Marine Syst., 68, 349–365, 2007. 2984

Meijer, P. Th., Slingerland, R., and Wortel, M. J. R.: Tectonic control on past circulation of the Mediterranean Sea: a model study of the Late Miocen, Paleoceanography, 19, PA1026, 1–19, 2004. 2985, 2993, 2994

Mellor, G. L. and Yamada, T.: Development of a turbulence closure model for geophysical fluid problems, Rev. Geophys., 20, 851–875, 1982. 2986

Mellor, G. L., Ezer, T., and Oey, L. Y.: The pressure gradient conundrum of sigma coordinate ocean models, J. Atmos. Ocean. Tech., 11, 1126–1134, 1994. 2986

Myers, P. G.: Flux-forced simulations of the paleocirculation of the Mediterranean, Paleoceanography, 17, 9–1, 2002. 2984

Myers, P. G., Haines, K., and Josey, S.: On the importance of the choice of wind stress forcing to the modeling of the Mediterranean Sea circulation, J. Geophys. Res.-Oceans, 103, 15729–15749, 1998a. 2984, 2987

Myers, P. G., Haines, K., and Rohling, E. J.: Modeling the paleocirculation of the Mediterranean: the Last Glacial Maximum and the Holocene with emphasis on the formation of sapropel S1, Paleoceanography, 13, 586–606, 1998b. 2984

Pérez-Asensio, J. N., Aguirre, J., Schmiedl, G., and Civis, J.: Impact of restriction of the Atlantic-Mediterranean gateway on the Mediterranean Outflow Water and eastern Atlantic circulation during the Messinian, Paleoceanography, 27, PA3222, doi:10.1029/2012PA002309, 2012. 2983

CC BY

Pratt, L. J. and Spall, M. A.: Circulation and exchange in choked marginal seas, J. Phys. Oceanogr., 38, 2639–2661, 2008. 2984
Roveri, M. and Manzi, V.: The Messinian salinity crisis: looking for a new paradigm?, Palaeogeogr. Palaeocl., 238, 386–398, 2006. 2982
Ryan, W. B. F.: Modeling the magnitude and timing of evaporative drawdown during the Messinian salinity crisis, Stratigraphy, 5, 227–243, 2008. 3006
Samuel, S., Haines, K., Josey, S., and Myers, P. G.: Response of the Mediterranean Sea thermohaline circulation to observed changes in the winter wind stress field in the period 1980–1993, J. Geophys. Res.-Oceans, 104, 7771–7784, 1999. 2984
Sannino, G., Bargagli, A., and Artale, V.: Numerical modeling of the mean exchange through the Strait of Gibraltar, J. Geophys. Res., 107, 9-1–9-24, 2002. 2984, 2985, 2989
Schneck, R., Micheels, A., and Mosbrugger, V.: Climate modelling sensitivity experiments for the Messinian Salinity Crisis, Palaeogeogr. Palaeocl., 286, 149–163, 2010. 2987
Seidenkrantz, M.-S., Kouwenhoven, T. J., Jorissen, F. J., Shackleton, N. J., and van der Zwaan, G. J.: Benthic foraminifera as indicators of changing Mediterranean–Atlantic water exchange in the late Miocene, Mar. Geol., 163, 387–407, 2000. 2981, 2982
Somot, S., Sevault, F., and Déqué, M.: Transient climate change scenario simulation of the Mediterranean Sea for the twenty-first century using a high-resolution ocean circulation model, Clim. Dynam., 27, 851–879, 2006. 2993, 2994
Sonnenfeld, P. and Finetti, I.: Messinian evaporites in the Mediterranean: a model of continuous inflow and outflow, in: Geological Evolution of the Mediterranean Basin, edited by: Stanley, D. J. and Wezel, F.-C., Springer, 347–353, 1985. 2983
Soria, J. M., Fernández, J., and Viseras, C.: Late Miocene stratigraphy and palaeogeographic evolution of the intramontane Guadix Basin (Central Betic Cordillera, Spain): implications for an Atlantic–Mediterranean connection, Palaeogeogr. Palaeocl., 151, 255–266, 1999. 2983
Stratford, K., Williams, R. G., and Myers, P. G.: Impact of the circulation on sapropel formation in the eastern Mediterranean, Global Biogeochem. Cy., 14, 683–695, 2000. 2994
Thompson, B., Nilsson, J., Nycander, J., Jakobsson, M., and Döös, K.: Ventilation of the Miocene Arctic Ocean: an idealized model study, Paleoceanography, 25, PA4216, doi:10.1029/2009PA001883, 2010. 2984
Topper, R. P. M. and Meijer, P. Th.: A modelling perspective on spatial and temporal variations in Messinian evaporite deposits, Mar. Geol., 336, 44–60, 2013. 2982, 2983

CPD
10, 2979–3026, 2014

Mediterranean response to gateway restriction

R. P. M. Topper and P. Th. Meijer

CC BY

Topper, R. P. M., Flecker, R., Meijer, P. Th., and Wortel, M. J. R.: A box model of the Late Miocene Mediterranean Sea: implications from combined $^{87}Sr/^{86}Sr$ and salinity data, Paleoceanography, 26, PA3223, doi:10.1029/2010PA002063, 2011. 2982

Tsimplis, M. N.: Vertical structure of tidal currents over the Camarinal Sill at the Strait of Gibraltar, J. Geophys. Res.-Oceans, 105, 19709–19728, 2000. 2989

Tsimplis, M. N. and Bryden, H. L.: Estimation of the transports through the Strait of Gibraltar, Deep-Sea Res. Pt. I, 47, 2219–2242, 2000. 2993

Tuenter, E., Weber, S. L., and Lourens, L. J.: The response of the African summer monsoon to remote and local forcing due to precession and obliquity, Global Planet. Change, 36, 219–235, 2003. 2981

van Assen, E., Kuiper, K. F., Barhoun, N., Krijgsman, W., and Sierro, F. J.: Messinian astrochronology of the Melilla Basin: stepwise restriction of the Mediterranean–Atlantic connection through Morocco, Palaeogeogr. Palaeocl., 238, 15–31, 2006. 2983

Weijermars, R.: Neogene tectonics in the Western Mediterranean may have caused the Messinian Salinity Crisis and an associated glacial event, Tectonophysics, 148, 211–219, 1988. 2983

Wessel, P. and Smith, W. H. F.: Free software helps map and display data, EOS Trans. AGU, 72, 441–446, 1991. 3008

Xu, X., Chassignet, E. P., Price, J. F., Özgökmen, T. M., and Peters, H.: A regional modeling study of the entraining Mediterranean outflow, J. Geophys. Res.-Oceans, 112, C12005, doi:10.1029/2007JC004145, 2007. 2989

Zavatarelli, M. and Mellor, G. L.: A numerical study of the Mediterranean Sea circulation, J. Phys. Oceanogr., 25, 1384–1414, 1995. 2985, 2986, 2991

CPD
10, 2979–3026, 2014

CC BY

Table 1. Overview of parameter values used to set up the model. SUIS = Smolarkiewicz iterative upstream scheme.

Parameter	Detail	Value
tprni	Inverse Prandtl number	0.2
horcon	Smagorinsky diffisivity coefficient	0.2
nitera	Number of iterations of the SIUS	2
sw	Smoothing parameter of the SIUS	0.8
t_E	External (2-D) time step	30 s
t_I	Internal (3-D) time step	1800 s
t_{RELAX}	Relaxation time scale of surface temperature forcing	1 day

CPD
10, 2979–3026, 2014

CC BY

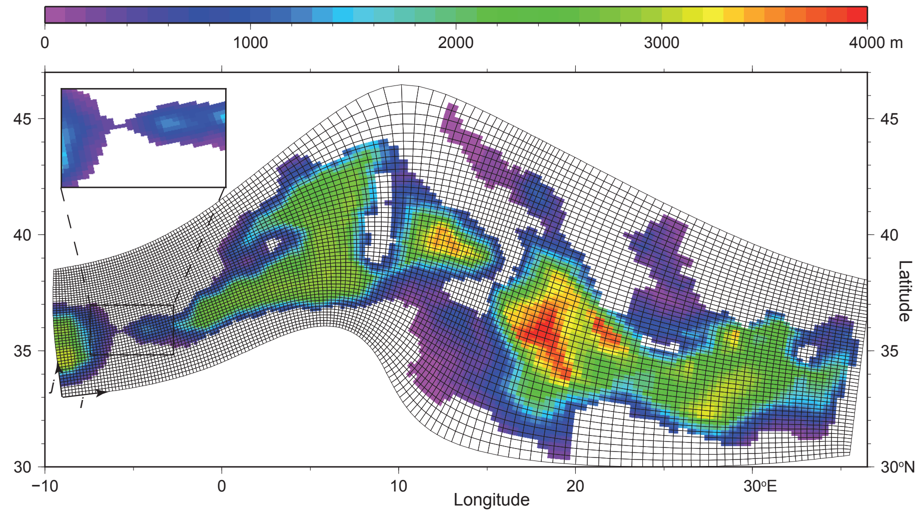

Figure 1. Model grid and bathymetry. Curvilinear grid coordinates i and j increase along curved lines towards, roughly, the east and north. The small inset shows the geometry of the Strait of Gibraltar in more detail.

CPD
10, 2979–3026, 2014

CC BY

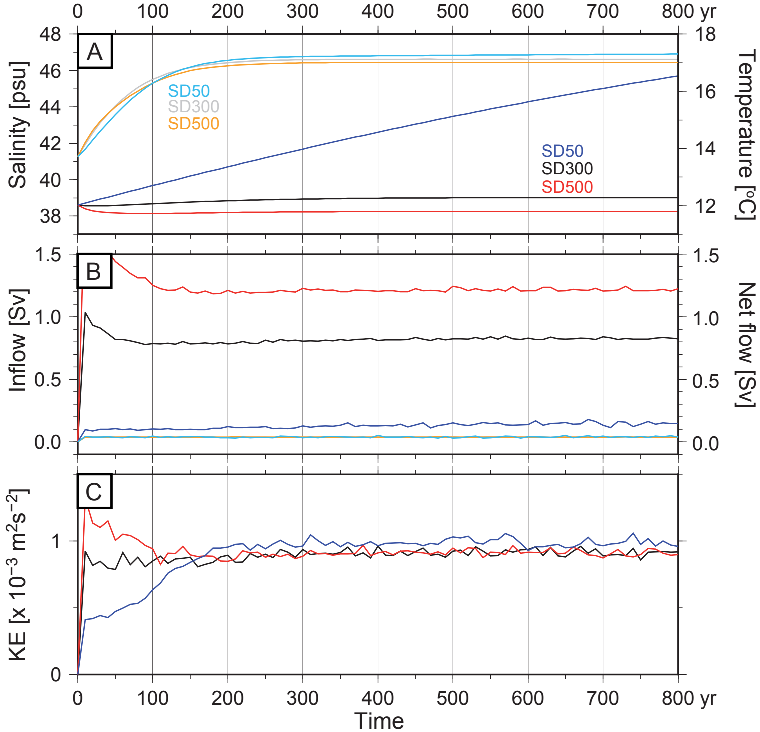

Figure 2. Temporal evolution of diagnostic variables for the reference experiments (SD300, black/grey lines), SD500 (red/orange) and SD50 (blue/lightblue). **(a)** Basin-averaged salinity (dark colours, left vertical axis) and basin-averaged temperature (light colours, right vertical axis). **(b)** Inflow (dark colours) and net flow (light colours) through the Strait of Gibraltar. **(c)** Kinetic energy measure.

CPD
10, 2979–3026, 2014

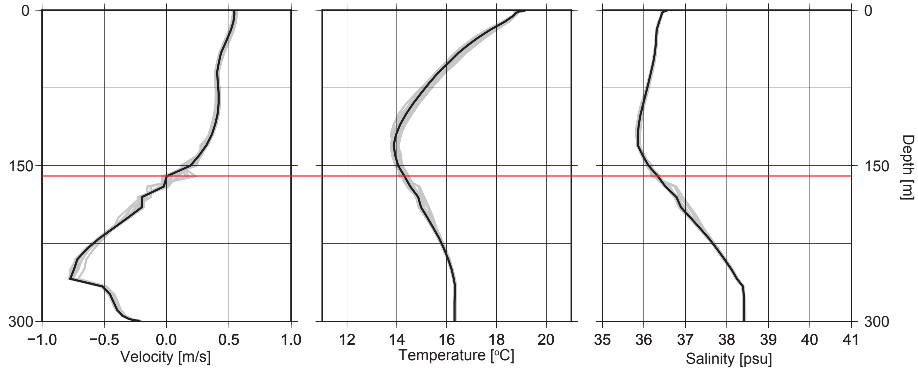

Figure 3. Vertical profiles of zonal velocity (left), temperature (middle), and salinity (right) in the middle of the Strait of Gibraltar in the reference experiment. Grey shading in each frame indicates the range of variation of the variable in the last 100 yr of integration, the solid black line is the average over the same 100 yr. The red line indicates the depth of the interface between inflow and outflow.

CPD
10, 2979–3026, 2014

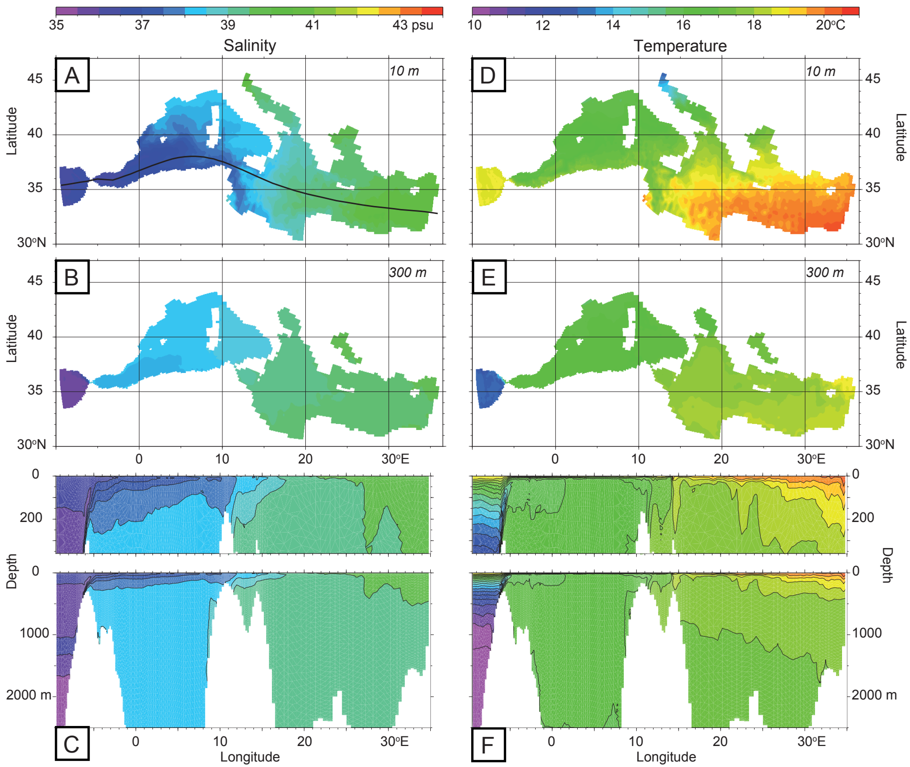

Figure 4. Two horizontal and a vertical cross section through the three-dimensional salinity **(a, c, e)** and temperature **(b, d, f)** fields averaged over the last 10 years of the reference experiment. Horizontal slices are shown in the surface layer (10 m) and at the sill depth of the Strait of Gibraltar (300 m). The vertical cross section is along the curved path indicated in **(a)** that crosses both the Gibraltar and Sicily straits.

CPD
10, 2979–3026, 2014

CC BY

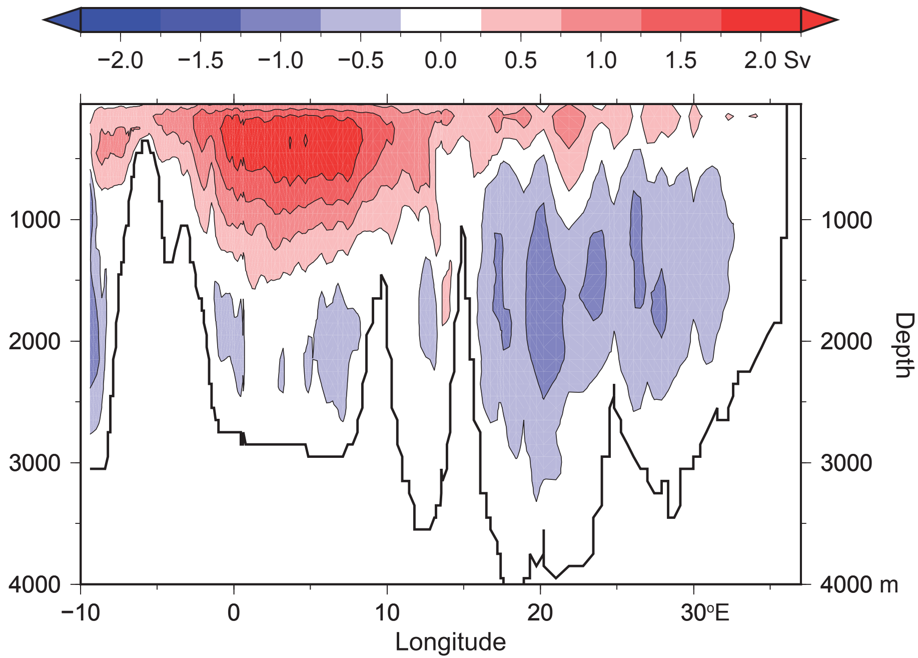

Figure 5. "Zonal" overturning stream function of the reference experiment. The contour interval is 0.5 Sv. Positive values (red colours) indicate clockwise circulation in this view, negative values (blue) anti-clockwise circulation.

CPD
10, 2979–3026, 2014

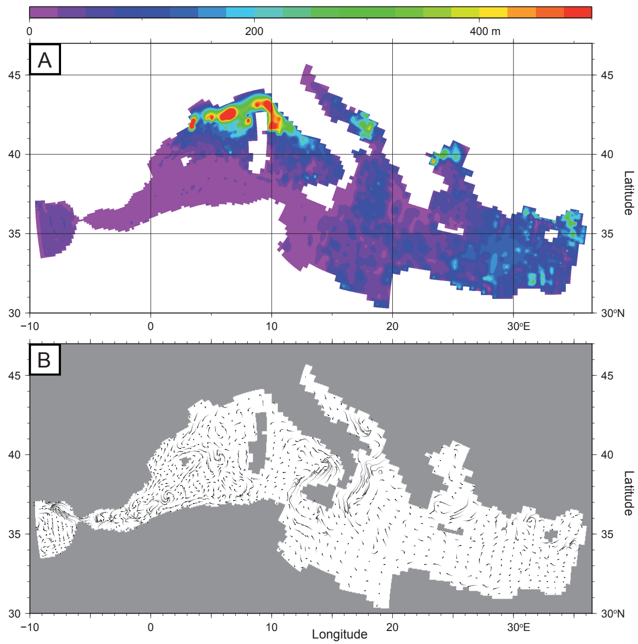

Figure 6. Mixed layer depth **(a)** and bottom currents **(b)** in the reference experiment. The mixed layer depth is defined as the depth, measured from the surface, of the minimum vertical mixing parameter. Bottom currents are visualized by tracking water particles for 30 days in the average velocity field of the last 10 years of integration. Trajectories start at light grey and proceed to black at the 30th day.

CPD
10, 2979–3026, 2014

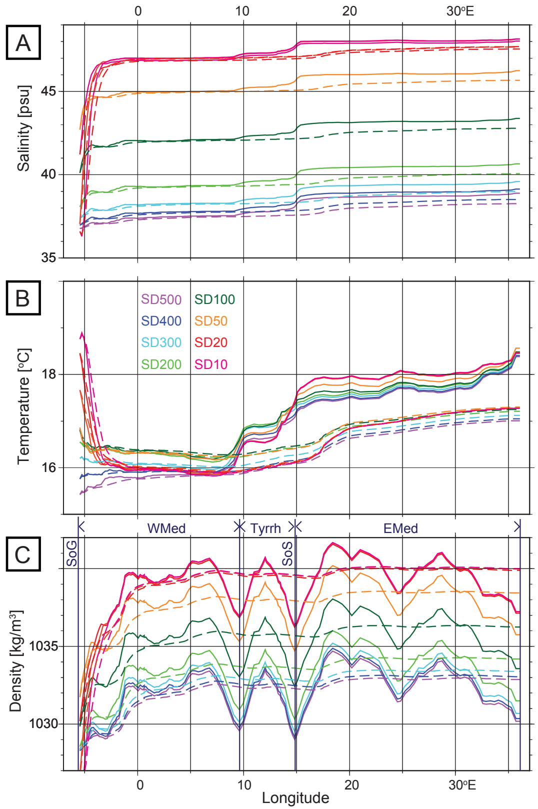

Figure 7. Latitude-depth-averaged profiles of salinity **(a)**, temperature **(b)** and density **(c)** for SD500–SD10. Dashed lines indicate the volume-averaged salinity/temperature/density of the volume between the Strait of Gibraltar and the indicated longitude. Therefore, the values at 36° E are the averages of the whole basin. Indicated in **(c)** are the longitudinal ranges corresponding to the western basin (WMed), the Tyrrhenian Sea (Tyrrh), and the eastern basin (EMed) and location of the Strait of Gibraltar (SoG) and Strait of Sicily (SoS).

CPD
10, 2979–3026, 2014

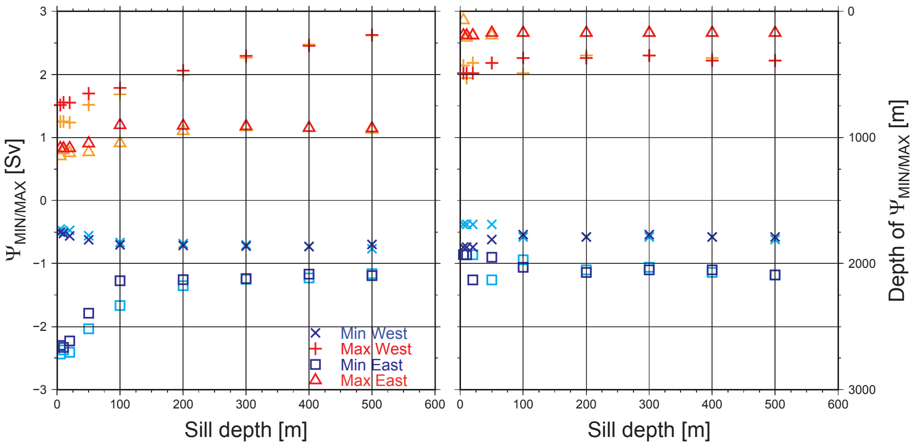

Figure 8. Strength (left) and depth of overturning extrema (right) of the upper (red) and deep (blue) zonal overturning cells in the western and eastern basin. To illustrate temporal changes, light colours indicate the value after 400 yr, dark colours the value after 800 yr.

CPD
10, 2979–3026, 2014

R. P. M. Topper and P. Th. Meijer

CC BY

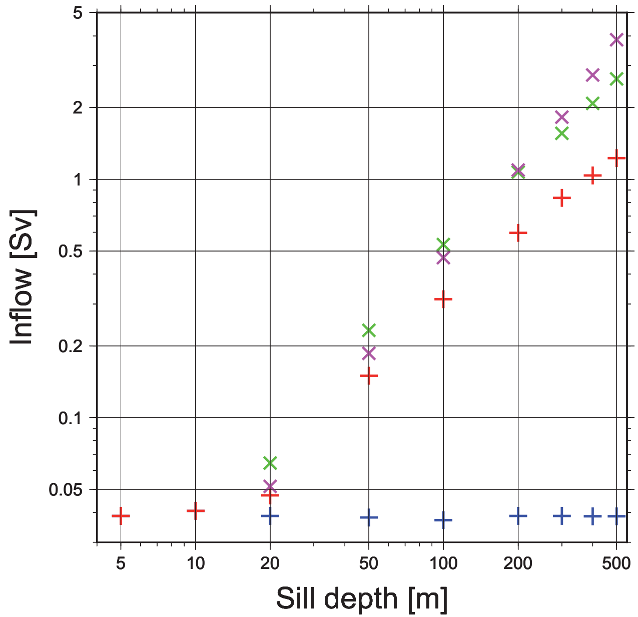

Figure 9. Modelled inflow (red plusses) and net flow (blue plusses) in SD500–SD5. Green crosses show the inflow calculated with hydraulic control theory from the basin-averaged densities of the Atlantic and Mediterranean. Purple crosses indicate the inflow calculated with hydraulic control theory using the average density of inflow and outflow in the gateway instead of basin averages.

CPD
10, 2979–3026, 2014

CC BY

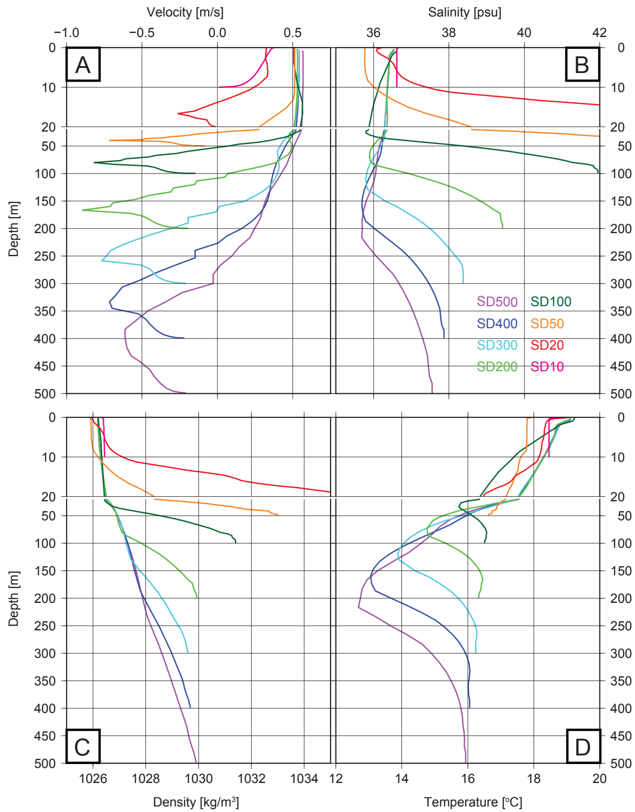

Figure 10. Vertical profiles of zonal velocity **(a)**, salinity **(b)**, density **(c)** and temperature **(d)** at the sill in the Strait of Gibraltar in experiments SD500–SD10. Note the change in vertical scale at 20 m. Temperature and salinity profiles of SD50 stand out with incongruent values near the surface. This is caused by a numerical overshoot due to steep slopes near the gateway in this experiment.

CPD
10, 2979–3026, 2014

R. P. M. Topper and P. Th. Meijer

CC BY